Analyst

Raman Mapping of Fentanyl Transdermal Delivery Systems with Off-Label Modifications

Journal:	*Analyst*
Manuscript ID	AN-ART-07-2019-001289.R1
Article Type:	Paper
Date Submitted by the Author:	21-Oct-2019
Complete List of Authors:	Xu, Teng; US Food and Drug Administration Yilmaz, Huzeyfe; U.S. Food and Drug Administration Willett, Daniel; U.S. Food and Drug Administration, ; Strasinger, Caroline; US Food and Drug Administration Rodriguez, Jason; Food and Drug Adm., Division of Pharmaceutical Analysis Keire, David; US FDA, Division of Pharmaceutical Analysis Wokovich, Anna; U.S. Food and Drug Administration

Raman Mapping of Fentanyl Transdermal Delivery Systems with Off-Label Modifications

Teng Xu[1], Huzeyfe Yilmaz[1*], Daniel R. Willett[1¥], Caroline Strasinger[2], Jason D. Rodriguez[1], David Keire[1], Anna M. Wokovich[1]*

[1] Food and Drug Administration (FDA)/Center for Drug Evaluation and Research (CDER)/Office of Pharmaceutical Quality (OPQ)/Office of Testing and Research (OTR)/Division of Pharmaceutical Analysis (DPA), St. Louis, Missouri

[2] FDA/CDER/OPQ/Office of New Drug Products (ONDP), Silver Spring, Maryland

* These authors contributed equally to this work

¥ Corresponding Author

E-mail: daniel.willett@fda.hhs.gov

Address: 645 S. Newstead Ave., St. Louis, MO 63110

This article reflects the views of the authors and should not be construed to represent Food and Drug Administration's views or policies.

Abstract

Raman mapping is a powerful and emerging tool in characterization of pharmaceuticals and provides non-destructive chemical and structural identification with minimal sample preparation. One pharmaceutical form that is suitable but has not been studied in-depth with Raman mapping are transdermal delivery systems (TDS). TDS are dosage forms designed to deliver a therapeutically effective amount of active pharmaceutical ingredient (API) across a patient's skin. To enhance drug delivery through the skin, the API in the formulation is often close to a saturated or supersaturated state. Thus, improper use or off-label modifications can lead to occurrence of unwanted API changes, specifically, crystallization over time. Here, off-label modifications were mimicked on a set of fentanyl drug-in-adhesive TDS sold on the U.S. market by four different manufacturers *via* die cutting, and then the die cut TDS were investigated through confocal Raman mapping for structural and chemical changes. Using Multivariate Curve Resolution (MCR), not only was morphological and chemical characterization of transdermal systems provided, but also fentanyl crystals in certain products due to off-label modifications were identified. The chemometric model used in analysis of Raman maps allowed precise identification of fentanyl as the crystalline material as confirmed by the hit-quality-index correlation of component spectra from the chemometric model with library spectra of fentanyl reference standard. The results show that confocal Raman mapping with MCR can be utilized in assessing pharmaceutical quality of TDS. This method has the potential to be widely used in characterization of such systems as an alternative to existing techniques.

Introduction

Raman mapping and imaging has been employed in analysis of various pharmaceutical systems such as solid forms, coatings and membranes, percutaneous delivery, microparticles, cells, and for drug dissolution testing.[1-8] However, for certain pharmaceuticals such as transdermal delivery systems (TDS), which are typically designed to have multiple homogeneous layers, confocal Raman mapping has not been fully utilized.[9, 10] TDS are most commonly drug-loaded, adhesive matrices applied to the skin which deliver a therapeutically effective amount of active pharmaceutical ingredient (API) to the systemic circulation.[11] To increase and sustain drug delivery over time, the concentration of the API in the TDS formulation is often made to be as close to or above the maximum drug concentration possible (i.e., a saturated or supersaturated solution).[12-15] Therefore, off-label modifications, improper handling or misuse of the drug product could cause the API to crystallize.[16]

The degree of crystallization is a critical quality attribute (CQA) for TDS because crystallized API within the TDS polymer matrix cannot pass through the skin, thus impacting therapeutic efficacy.[17] More specifically, crystallization reduces the amount of solubilized API thereby altering the concentration gradient between the adhesive matrix and skin, a critical element of the driving force for drug delivery *via* the transdermal route.[18] Furthermore, changes in the rheological properties of the drug-in-adhesive (DIA) matrix due to API crystallization may result in adhesion failures that effectively reduces the surface area of the TDS that is in contact with skin and may further decrease the total amount of drug delivered to the patient. Overall, failure to control crystallization results in poor product quality and could result in poor patient outcomes. For example, there have been several recalls of TDS due to quality issues associated with crystallization. In 2008, Neupro® (rotigotine) transdermal system, a product for the treatment of the signs and symptoms of early-stage idiopathic Parkinson's disease was recalled

and discontinued because of rotigotine crystallization.[19] In addition, in 2012, one lot of Duragesic 25 mcg/h (a fentanyl TDS) was recalled because of fentanyl crystallization.[20] These two incidents highlight the need to develop analytical approaches capable of evaluating the potential for crystallization in TDS products.

Currently, optical microscopy, infrared spectroscopy, differential scanning calorimetry (DSC) and X-ray diffraction (XRD) are used to characterize the size, distribution and other physio-chemical properties of crystals formed in TDS.[18, 21-33] Although optical microscopy provides rapid and non-destructive size and distribution information, it cannot identify chemical properties of crystals forming in an adhesive matrix. Another limitation of optical microscopy is due to the TDS matrix, which typically consists of three main layers (release liner, drug-in-adhesive layer and a backing film) with similar refractive indices, making crystals difficult to optically resolve from the matrix. While chemical properties of crystals in TDS can be obtained by infrared spectroscopy, DSC and XRD, challenges such as adhesive matrix interference and sparse distribution of crystals in the TDS persist.[22, 24, 26, 27, 33, 34] Moreover, these techniques require separation of the crystals from the matrix for analysis, which is an additional challenge. Hence, there is a need for non-destructive, chemical and structural analysis methods for improving both the manufacturing of TDS as well as analysis for monitoring the stability of the finished product. Here, the use of confocal Raman mapping is evaluated for assessment of TDS quality, specifically for identification and analysis of crystals formed from the API.

Raman spectroscopy is an effective technique in chemical identification as the technique provides molecular fingerprint information by measuring vibrational or rotational energies of chemical bonds.[35] For pharmaceutical analysis, Raman can be used to determine composition, diffusion and distribution properties of APIs and excipients, which are important in drug

development or finished product testing.[36-38] To investigate spatial and spectral features of a pharmaceutical sample with high-resolution, Raman spectroscopy may be coupled with confocal microscopy, where scattered light from outside of a small focal area is blocked by an aperture. A representative analysis of a drug product can then be achieved by performing a point mapping across the area of interest.

Large area scans have become achievable with recent advancements in light sources, spectrometers and spatial control systems, empowering rapid and high-resolution Raman mapping of pharmaceuticals.[38] To obtain a chemical/structural image from a Raman dataset, statistical analysis of the map provides the best results.[39] The simplest approach is based on assigning peaks in vibrational spectra to molecules of interest to obtain spatial and chemical information about them. Although such methods are useful in qualitative and quantitative Raman mapping more sophisticated multivariate statistical methods, utilize spectral information more effectively and allow in-depth analysis without the *a priori* knowledge regarding assignment of Raman peaks. Therefore, when constructing visuals for Raman mapping, multivariate statistical methods such as Principal Component Analysis (PCA), Classical Least Squares (CLS), Multivariate Curve Resolution-Alternating Least Squares (MCR-ALS) or Partial Least Squares (PLS) are commonly employed.[2, 40, 41 42]

Here, a non-destructive analytical method for characterization of TDS based on confocal Raman mapping and MCR-ALS analysis was developed. Four commercially-available 25 µg/hr drug-in-adhesive fentanyl TDS sold on the U.S. market by different manufacturers (labeled here as TDS-1, TDS-2, TDS-3, and TDS-4) were used. The TDS were first modified *via* die-cutting and then aged for approximately one year to promote crystallization. A yearlong aging time was used because this is within the typical expiry of TDS and because of the relatively low ion

activities and diffusion rates of APIs in polymer matrices that can prevent immediate crystallization.[43] Storage of samples for a period of 1 year at ambient conditions (within the per-label storage range of 20 ˚C to 25 ˚C) was to emulate traditional patient or caregiver practices.[44] Die-cutting exposed a fresh edge of the samples to ambient conditions and allowed for the simulation of typical off-label modifications, such as cutting the TDS into smaller pieces to administer smaller dosages or damages in defective TDS.[45, 46] Unmodified TDS samples were included in the study to serve as control samples. The areas around the die-cut region where fentanyl crystals could possibly form were mapped using confocal Raman microscopy. Assuming a uniform and homogeneous adhesive layer in the TDS, the crystallization was investigated through variation in the vibrational spectra and analyzed via a two-component MCR-ALS method. With MCR-ALS multivariate analysis, chemical fingerprints were used to identify fentanyl crystals in certain TDS. Since the most prominent Raman feature of fentanyl is common in various fentanyl analogues[47], a more comprehensive identification was achieved by comparing the MCR-ALS components relating to fentanyl crystals with USP reference standard fentanyl spectra. Using the correlative hit-quality-index (HQI) as a figure of merit, the MCR-ALS components of the fentanyl crystals in the Raman mapping analysis were found to have HQI values larger than 0.95, which has been used as a threshold for pass or fail determinations in other studies.[48]

Materials and Methods

Materials

Fentanyl reference standard was purchased from U.S. Pharmacopeia Convention (USP) and used "as is". Four commercially-available 25 μg/hr drug-in-adhesive fentanyl TDS products (TDS-1, TDS-2, TDS-3, and TDS-4) were purchased. The properties of these four TDS are summarized in Table 1. Unmodified TDS were examined and tested immediately after opening their sealed pouch. Aged TDS were first cut with a 7 mm diameter arch punch and then stored unsealed at room temperature for over 12 months before analysis.

Table 1. **Summary of TDS properties**

	Active Ingredient	Dosage Strength (μg/hr)	API Amount (mg)	Inactive Ingredients
TDS-1	Fentanyl	25	2.76	Polyethylene terephthalate backing film, polyisobutene adhesive, isopropyl myristate, octyldodecanol and polybutene
TDS-2	Fentanyl	25	4.2	Ethylene vinyl acetate/polyethylene terephthalate backing film, polyacrylate adhesive and isopropyl myristate
TDS-3	Fentanyl	25	2.55	Polyolefin backing film, silicone adhesive and dimethicone NF
TDS-4	Fentanyl	25	2.55	Polyethylene/polyester backing film, polyisobutylene adhesive, mineral oil, isopropyl myristate

Methods

API crystallization, microstructure and chemical properties of all eight TDS with and without die-cutting and aging were characterized by StreamHR^{TM} Raman imaging using a Renishaw InVia confocal Raman microscope. A 785 nm laser excitation source, -70 ºC thermoelectrically cooled charge-coupled device (CCD) camera and a Leica DM2500

microscope with 50x / NA 0.75 objective were used for Raman spectroscopy acquisition. A 1200/mm grating was used to disperse the light through a spectral range of 400-1500 cm^{-1}. A 3.0 μm step size was used with exposure time of 10 seconds scanning through a 510 ×441 μm area. For unmodified TDS, the area of interest was selected away from the edge. For the die-cut and aged TDS, the investigation area was selected near the cut edge. The laser was focused on the surface of the TDS to mitigate the interference from the backing film. Raman mapping and MCR were used to study the component distributions in complex TDS matrices. WiRE 4.4 and Matlab R2017a with PLS Toolbox were used for spectral pre-processing and MCR analysis. The Raman maps of the TDS were pre-processed to reduce non-chemical effects that can attribute to spectral variance. Cosmic ray removal was done in WiRE 4.4 software using the width of feature and nearest-neighbor methods. The data was imported[49] into Matlab R2017a and pre-processing and MCR analysis of the data was then carried out using PLS Toolbox + MIA (Eigenvector Research, Inc., Version 8.6.2). The spectral region was restricted to 400 to 1560 cm^{-1}. Data preprocessing only included baseline correction with a Whittaker filter (asymmetry=0.001, lambda=100).

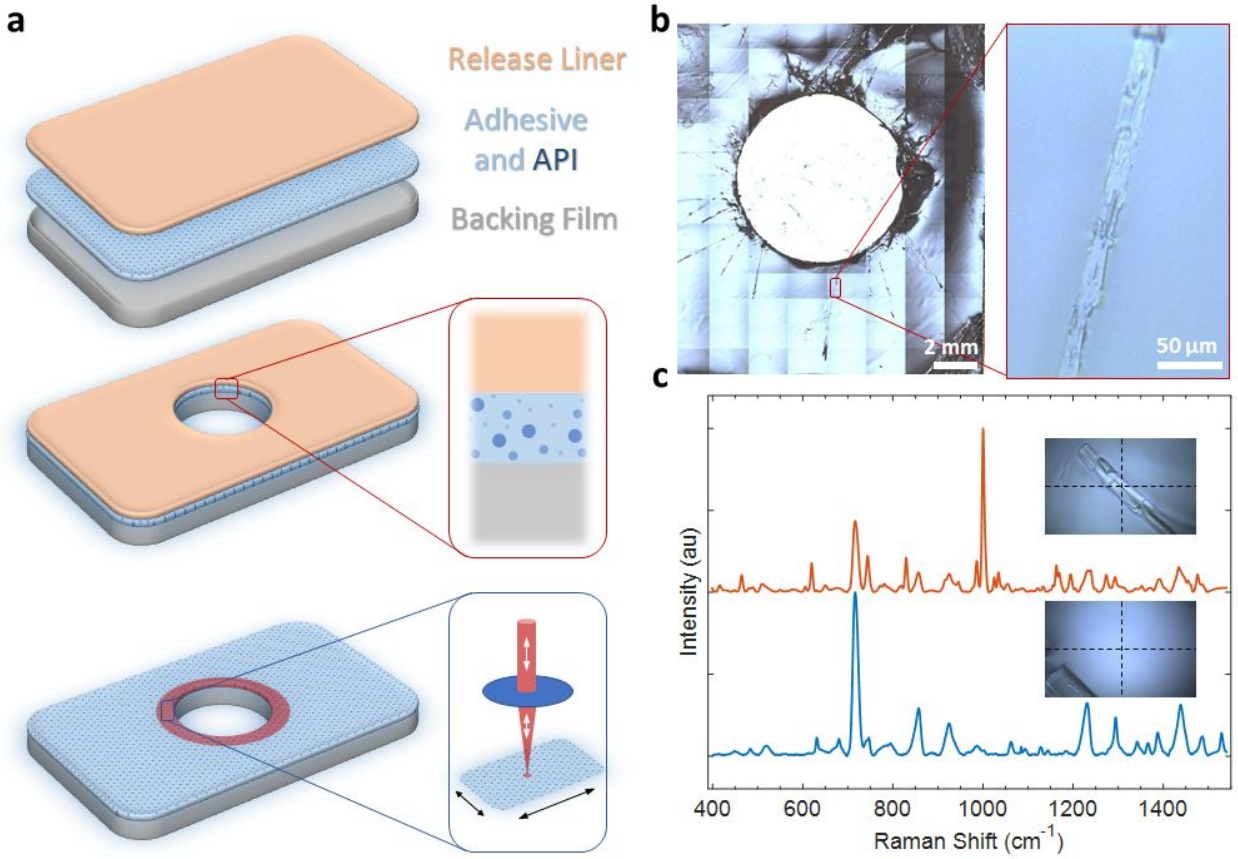

Figure 1. The schematic for TDS (top) and the experimental procedure involving die-cutting (middle) and Raman mapping (bottom) (a). Crystal formation and proliferation around the die-cut region after aging for longer than 12 months at 5X (left) and 100X (right) magnifications (b). Raman spectra from crystalline and non-crystalline regions overlaid to demonstrate the significant differences in peak positions and intensities (c).

Result and discussion

The overall experimental procedure included several steps as illustrated in Figure 1a. First, fentanyl TDS were die-cut and aged for more than 12 months. The cutting of the TDS was performed to mimic the cutting that may be done by a healthcare provider or patient prior to administration. The adhesive layer not only incorporates the API, but also contains several other chemicals used in the making of the adhesive as well as for stabilizing the API. Die-cutting exposes the adhesive layer to ambient conditions where modifications in adhesive layer composition due to evaporation and other possible effects could cause crystallization of the API. The areas around the die-cut region were then inspected for possible crystal formation or any other kind of non-uniformity (Figure 1a). This experimental design was successful in generating crystals in TDS-4, where crystal proliferation was observed around the die-cut areas (Figure 1b). Such suspect areas were identified using optical microscopy and inspected with confocal Raman microscopy. The Raman spectra of regions with and without crystals were visually observed to be different. Specifically, a strong peak around 1001 cm^{-1} (observed in Raman spectra of pure fentanyl) was observed which was indicative of the crystal structure being like that of pure fentanyl (Figure 1c). Subsequently, the experimental procedure was applied systematically to the four fentanyl TDS with and without die-cutting or aging applied as an off-label modification.

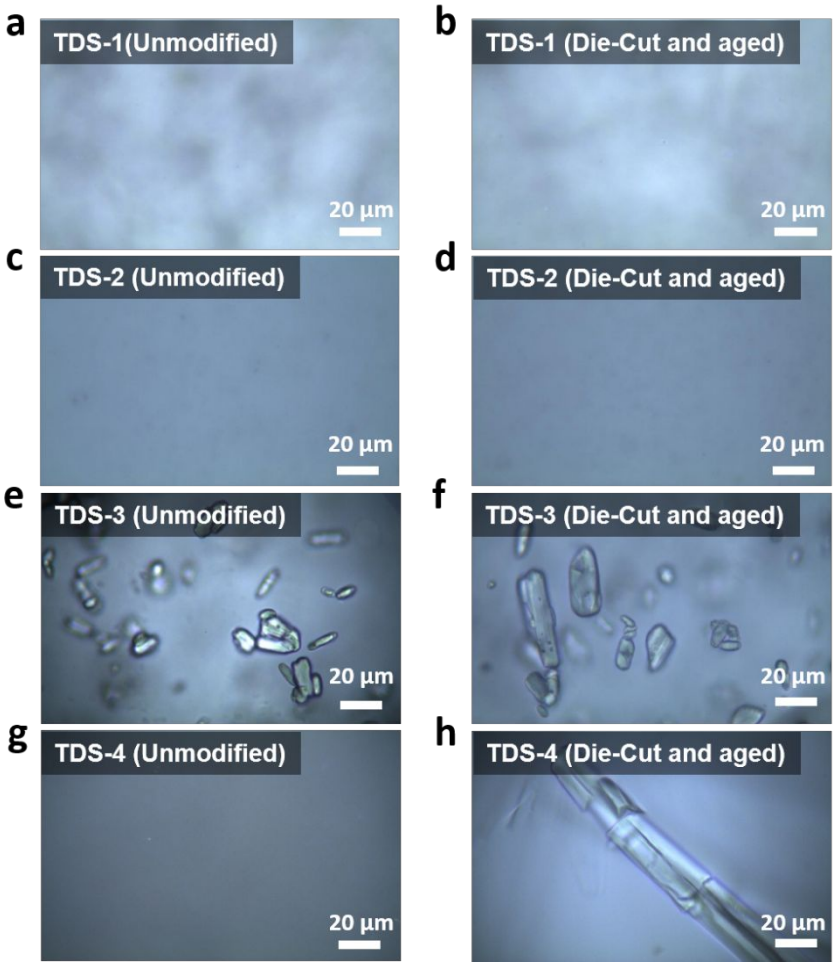

Figure 2. Optical image of TDS-1 unmodified sample (a), die-cut and aged sample (b); TDS-2 unmodified sample (c), die-cut and aged sample (d); TDS-3 unmodified sample (e), die-cut and aged sample (f); TDS-4 unmodified sample (g), die-cut and aged sample (h). The scale bars are 20 µm.

Microstructure of TDS

Microstructures of all four unmodified and die-cut and aged TDS samples were characterized by optical microscopy as shown in Figure 2. Each optical image was taken at the surface of the DIA layer and inspected. The images showed similar microstructures for TDS-1 with or without die-cutting and aging. The non-uniform background in the optical images of TDS-1 can be attributed to light scattering from the rough surface of the backing film under the semi-transparent DIA layer. Similarly, the microstructures of TDS-2 with or without die-cutting and aging were similar, and no crystallization was observed in either TDS-1 or TDS-2. By contrast, small (< 50 μm in length) crystals were observed in the DIA matrix both with or without die-cutting and aging in TDS-3. Overall, die-cutting and aging did not induce significant changes in TDS-1, TDS-2 or TDS-3, and DIA layers in these transdermal systems were not affected according to visual observation.

The microstructure of the unmodified TDS-4 sample showed a homogenous microstructure. Notably, in modified and aged (12 months) TDS-4, large elongated fentanyl crystals (approximately 20 μm wide and up to ~5 mm long) were observed emanating from the edge of die cut areas. This suggested that the cutting process had initiated crystallization. A time-lapse study of crystal growth in TDS-4 was also conducted (Figure S1). While all TDS samples analyzed in this study were aged for a period of 1 year, the time-lapse study provided confirmation for the proliferation of crystals from the die-cut edges.

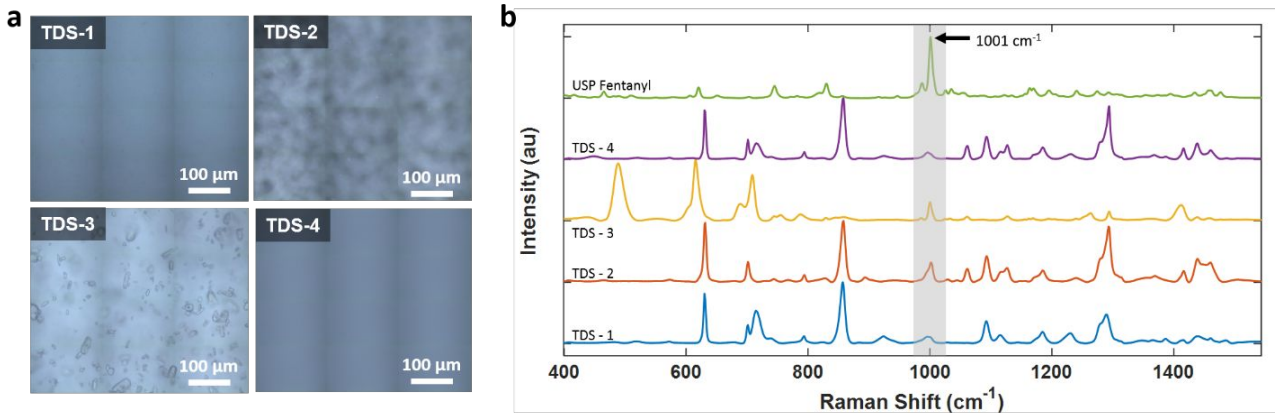

Figure 3. Optical image of the TDS areas investigated with Raman microscopy in unmodified samples (a); reference standard (USP) fentanyl spectrum (green) and mean spectra of TDS-1 (blue), TDS-2 (orange), TDS-3 (yellow) and TDS-4 (purple) (b). Scale bars are 100 µm.

Raman spectroscopy analysis of TDS

As shown in Table 1, there are three different pressure-sensitive adhesives used in the four TDS formulations studied here. Polyacrylate adhesive was used in TDS-2, polyisobutene adhesive was used in TDS-1, polyisobutylene adhesive was used in TDS-4, and silicone adhesive was used in TDS-3. While polyacrylate has a higher fentanyl solubility compared to polyisobutene, polyisobutylene and silicone,[50] silicone has several advantages over other adhesives, such as low skin irritation and excellent API diffusivity properties.[51] However, poor solubility of APIs or other excipients can lead to formation of crystals in TDS incorporating silicone within their adhesive matrix.[52] Therefore, crystallization observed in TDS-3 (Figure 2e, 2f and 3a) may be attributed to the relatively low fentanyl solubility in silicone adhesive.

Raman spectra of reference standard fentanyl is shown in Figure 3b. The signature peak of fentanyl at 1001 cm^{-1} is associated with υ (C-C) aromatic ring-breathing (Figure S2). To compare the Raman spectra of the fentanyl reference standard with fentanyl transdermal delivery systems, the mean spectra of all unmodified TDS samples (Figure 3a) collected over an area of

510 μm × 441 μm (see methods for details) were plotted and are shown in Figure 3b. All the TDS displayed the signature fentanyl peak at 1001 cm^{-1}, as well as Raman signatures from other ingredients that make up the DIA matrix and the backing film. Since a confocal system with a 50× objective that has a depth-of-focus of 3 μm was used, and the thickness of the DIA layers in fentanyl TDS varied between 20-100 μm (Figure S6), the DIA layer was primarily probed. However, Raman signatures from the backing film were present since the DIA layer was transparent and allowed propagation into the samples. At first glance, Raman spectra of TDS-1, TDS-2 and TDS-4 were similar to each other as they displayed peaks at 631, 858, 1183 and 1294 cm^{-1}. The similarity of spectra from TDS-1, TDS-2 and TDS-4 can be attributed to polyethylene terephthalate (PET) in the backing film which was responsible for these peaks in the spectra.[53] However, TDS-3 had a different spectrum with peaks at 489and 709 cm^{-1} that are associated with υ(Si-O-Si) symmetric stretching and υ(C-Si-C) symmetric stretching. Because silicone adhesive is a copolymer synthesized by a condensation reaction between polydimethylsiloxane (PDMS) and a silicone resin, the presence of PDMS in the TDS-3 (Table 1) can account for the observation of the peaks at 489 and 709 cm^{-1}.[54, 55] Furthermore, polyolefin backing film in TDS-3 manifests as peaks at 1295 and 1415 cm^{-1}.[56]

On the other hand, peaks located at 716, 1230 and 1439 cm^{-1} in TDS-1 and TDS-4 were attributed to polyisobutylene and polyisobutene adhesives which have been widely used in TDS due to their chemical inertness and low cost. Similar to the use of silicone in DIA layer, use of polyisobutene and polyisobutylene also offers poor solubility for API and other excipients.[57, 58] However, the desired adhesive and viscoelastic properties can be achieved by either the combination of low and high molecular weight polybutylenes or incorporation of tackifiers such as polybutenes (e.g., as an excipient used in TDS-1) and plasticizers such as mineral oil (e.g., as

an excipient used in TDS-4).[58] Notably, TDS-1 and TDS-4 both use isopropyl myristate (IPM) as a penetration enhancer but showed very different results with off-label modifications. These results suggest that fentanyl crystallization in die-cut and aged TDS-4 may be associated with the lack of stabilization by a crystallization inhibitor, such as the octyldodecanol present in the TDS-1 formulation but absent in TDS-4. Note that, although IPM and mineral oil were present in TDS-4, they were not differentiated since they had overlapping Raman peaks with the ingredients of the backing film.[59] The Raman spectra of inactive ingredients are also provided in the supporting information (Figure S7) to serve as a reference for the association of the peaks mentioned above.

Based on the Raman spectroscopy results detailed above, Raman mapping was performed on all four unmodified and die-cut and aged TDS samples. Because the TDS consist of a thick backing film and a thin DIA layer, confocal Raman spectra contained signatures from both layers. In addition, as DIA layers in TDS contain various chemicals for API stabilization, adhesive efficiency and diffusion rate control, mean Raman spectra of TDS contained many peaks. However, when compared with the fentanyl reference standard, despite the presence of the peak at 1001 cm^{-1} associated with υ (C-C) aromatic ring-breathing in fentanyl, all four TDS spectra contained several different peaks and were easily distinguishable from pure fentanyl. This fact constituted the basis for the mapping analysis. By utilizing the Raman spectra collected over the areas shown in Figure 3a in the multivariate analysis, fentanyl crystals forming in the adhesive matrix were chemically and structurally identified.

Raman mapping of TDS

API crystal size and distribution are critical quality attributes (CQA) for drug-in-adhesive TDS and Raman mapping allows chemical characterization of these CQA. However, to visualize

crystal size and distribution in a 2-dimensional Raman map, dimensionality reduction of spectral information is required. To do this, *a priori* physio-chemical information can be used on the Raman spectra and by calculating the predominant peak position, area, intensity or integration, spectral information can be reduced to a single data point. However, such methods fail when the predominant peak is not selective enough for precise identification, or when evolution of the API through interactions with excipients in the adhesive matrix of TDS leads to unexpected forms. Multivariate analysis can reduce the spectral data and provide visual characterization by utilizing multiple Raman bands without *a priori* physio-chemical information. In addition, since multivariate analysis of Raman maps are based on variance, not only can unwanted forms be detected, but they can also be thoroughly identified with adequate methods. Here, we present such comprehensive characterization of commercially available fentanyl TDS with and without off-label modifications, using confocal Raman mapping and multivariate analysis.

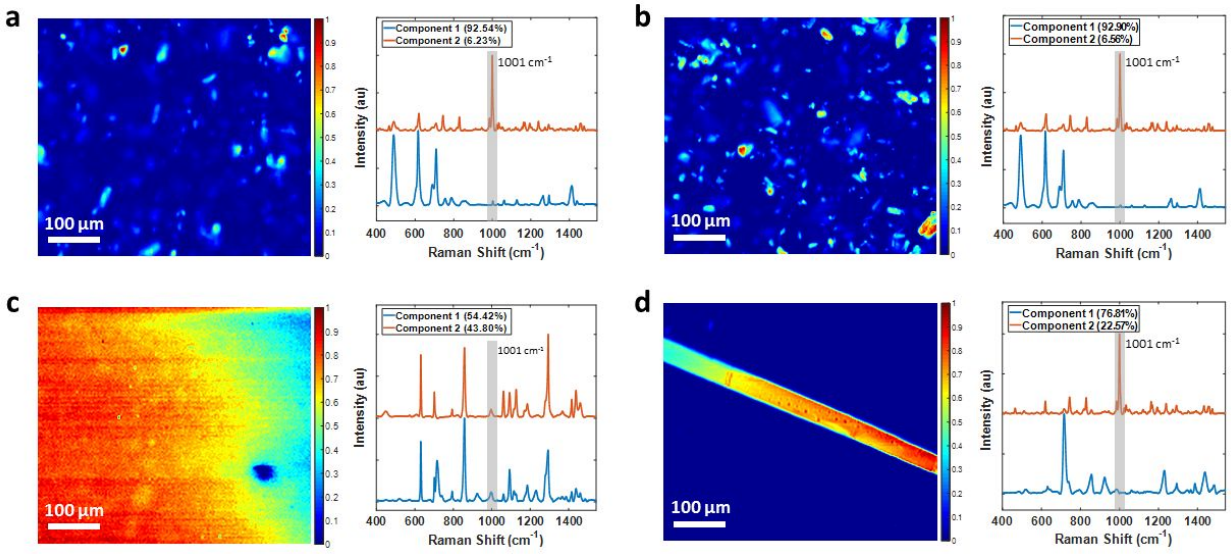

Figure 4. Confocal Raman image of the second components (left) and spectra of the two components (right) of unmodified TDS-3 (a), die-cut and aged TDS-3 (b), unmodified TDS-4 (c) and die-cut and aged TDS-4 (d). Scale bars are 100 µm.

Raman spectra collected over an area of 510 ×441 µm at 3 µm step sizes constituted a

dataset with 25,308 spectra and 1,011 spectral points (400-1550 cm^{-1}). To construct Raman maps of the TDS, the simplest approach would be to integrate the predominant 1001 cm^{-1} Raman signature of fentanyl. However, the fentanyl peak at 1001 cm^{-1} is due to aromatic ring breathing and does not fully characterize the suspect structures as fentanyl crystals. Fentanyl is a highly potent analgesic API that has numerous analogues that manifest the exact same predominant Raman peak.[60] Therefore its precise and thorough characterization is paramount for the safety and efficacy of TDS. Also, by relying on a single Raman peak, polymorphic changes or co-crystallization that could potentially occur may be overlooked due to that single peak being also present in these spectra. On the other hand, with multivariate methods, spectral features are utilized fully by exposing the variance within a spectral map and, simultaneously, dimensionally reducing the dataset. Typically, unsupervised methods such as Principal Component Analysis (PCA) are used for chemical imaging/mapping which perform the task *via* eigen decomposition of the covariance of the spectral dataset. However, eigenvectors that are used in the dimensionality reduction are not true representatives of the Raman spectra, rather, they represent the contribution of a mixture of the Raman signatures (peaks) to the spectral variance. To obtain the spectral information of unknown or unwanted forms or structures of the API in a complex TDS by chemical mapping, a better suited method is Multivariate Curve Resolution-Alternating Least Squares (MCR-ALS). In this work, MCR-ALS was applied to Raman mapping with the assumption of a two-component system. Since a confocal Raman microscope was employed to map a uniform adhesive layer (the first component), any non-uniformity (i.e., crystallization) was expected to manifest as the only other component in the dataset.

A brief description of the MCR-ALS analysis and details of its implementation is presented in the following paragraphs.

Within the broader spectroscopy context, MCR-ALS as a statistical technique is most useful for retrieving spectral information of pure components in mixture spectra where the components are unknown, or their spectral information is not available. Hence, MCR-ALS tools have been developed on various platforms and employed for imaging/mapping analysis of spectroscopic measurements.[61-64] Briefly, recovery of pure components by MCR is performed by solving the following mathematical problem:

$$D = CS^T + E \quad (1)$$

where D is the dataset of interest, C is the matrix representing contributions (concentrations), S is the matrix of pure component spectra and E is the residuals matrix, ideally representing the experimental error.[65, 66] An effective way to solve this problem is to use ALS which is a two-step, iterative optimization method. The two steps in ALS are (i) initialization of either the concentrations matrix or the pure component matrix and (ii) careful selection of convergence parameters. In this work, the initialization of the ALS was achieved by assuming that the pure components were within the dataset. Pure components (adhesive matrix and formed crystal in this work) were calculated by locating the points on the exterior of the normalized data space.[67] For convergence, 300 maximum iterations were used with a convergence tolerance of 10^{-8} change in the fit. While the fit of each component is shown in Figures 4 and S3, uncertainty of the MCR-ALS model from each dataset was calculated and is shown in Table-2. The residuals maps and loadings for each TDS sample are shown in Figures S4-5. The only constraint applied to the MCR-ALS model was non-negativity which is a natural assumption in vibrational spectroscopy.

Based on the MCR-ALS analysis, Raman maps of the four unmodified TDS products and their die-cut and aged counterparts were generated as shown in Figure 4 and Figure S3. In cases

where no fentanyl crystallization was observed (TDS-1 and TDS-2), variation within the Raman spectra of the mapped area was due to the divergence of the TDS under the microscope (Figure S3). Spectral variations in TDS-1 and TDS-2 were analyzed by inspecting the MCR components since Raman signatures of ingredients in backing film layer and DIA layer were observed at varying intensities. The relative intensities of peaks at 631, 858, 1183 and 1294 cm^{-1} compared with that of peaks at 716, 1230 and 1439 cm^{-1} were different (Figure S3 a-b) in TDS-1. Recall that, the first set of peaks are associated with the backing film (PET) in TDS-1, TDS-2, and TDS-4, where the second set of peaks are associated with the DIA layer (section 3.2) of TDS-1. Similarly, component spectra of TDS-2 only displayed variations among the backing film and the DIA layer. The main difference between the two estimated components of TDS-2 was the variation of the relative intensities of the polyacrylate adhesive signature peak at 1439 cm^{-1} and fentanyl peak at 1001 cm^{-1} compared with that of the backing film peaks at 631, 858, 1193 and 1294 cm^{-1} (Figure S3 c-d). Given the large TDS area that was interrogated with confocal Raman microscopy, using a 50× objective and the shape/size of the transdermal systems, a gradient change in the focal point of the microscope with respect to the transdermal system on the stage was not unexpected. Such a gradient in the distance between the microscope and the sample can explain the chemical structures observed in the MCR-ALS analysis of maps of TDS-1 and TDS-2 with or without off-label modifications.

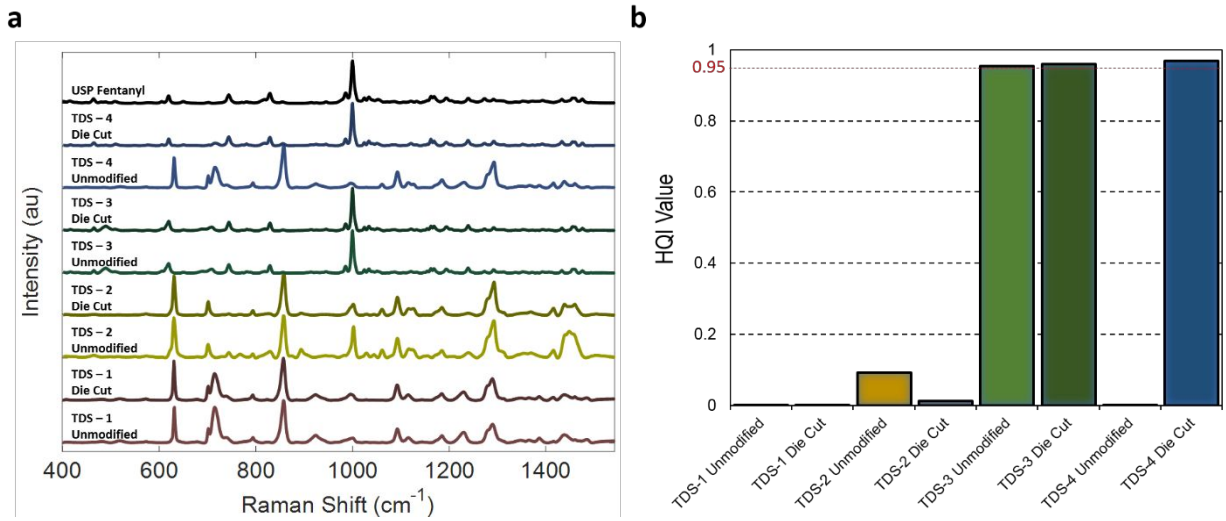

Figure 5. Estimated spectra (a) and the calculated HQI values of the second pure components of all TDS.

As for the transdermal systems where pre-existing fentanyl crystals were observed (TDS-3) or crystallization of fentanyl was initiated with die-cutting (TDS-4), pure component spectra captured the variance among the crystal structures of fentanyl and the overall TDS (Figure 4). In TDS-3, crystal structures observed by optical microscopy and demonstrated in Figure 2e and Figure 2f were analyzed with the two component MCR-ALS method. Because the images of the two components are complementary to each other, only the Raman images of the second components are shown for all TDS studied here (Figure 4 and Figure S3). Importantly, Raman mapping and MCR-ALS analysis of TDS-3 showed that small fentanyl crystals existed in both unmodified and die-cut samples, however, showed no crystal growth in their relative size and number. Note that, certain silicone-based fentanyl TDS are formulated by suspending fentanyl particles in solvated silicone adhesives[68]. Since TDS-3 was formulated with a silicone adhesive, presence and stability of fentanyl crystals can pertain to a similar formulation strategy.

For both the unmodified and die-cut TDS-3 Raman maps, estimated pure component spectra were very similar as shown in Figure 4 a-b. In addition, the spectra of the first component

displayed the same peaks with similar relative intensities as the mean spectrum of TDS-3 shown in Figure 3 (see section 3.2 for details). More importantly, the spectra of the second component was similar to the reference standard fentanyl spectrum. Similarity of all the TDS was quantitated using a correlative method as described in Section 3.4.

TDS-4 was the only product that was significantly affected by the die-cutting process. MCR-ALS analysis of the Raman mapping of the unmodified TDS-4 sample only captured variance between the DIA layer (adhesive) and the backing film layer. As shown in Figure 4c (right), Raman peaks at 716, and 1230 cm^{-1} associated with polyisobutylene adhesive were prominent in the first component and were absent in the spectrum of the second component. Similar observations were made for TDS-1 and TDS-2 (Figure S3), and, as described above, attributed to the change in the distance between the focal point of the Raman microscope and the DIA layer causing variations among the spectra of the area mapped. However, large crystals that proliferated from the die-cut area in TDS-4 after aging (also shown in Figure 2h) could be assigned as fentanyl crystals because the second pure component spectrum displayed the same Raman signatures as the reference standard fentanyl spectrum (Figure 4d). Note that, the spectrum of the first component in Figure 4d (die-cut TDS-4) differs from that of the unmodified TDS-4. The difference is attributed the focal point of the confocal Raman microscope being adjusted for the larger crystal that had proliferated out of the transdermal system plane. Notably, the Raman signatures observed in Figure 4d-right (716 and 1230 cm^{-1}) are from the polyisobutylene adhesive and only the Raman signatures of the backing film (631, 858, 1183 and 1294 cm^{-1}) are absent. This is consistent with the focal point being further from the backing film as the beam is focused on the proliferated crystal. Table 2 summarizes the outcomes of the multivariate analysis assisted Raman mapping study of fentanyl TDS products studied here.

Table 2. Summary of Results

Product	Raman Bands from Backing Films (cm^{-1})	Raman Bands from Drug-in-Adhesive Layers (cm^{-1})	Raman Mapping and MCR-ALS Conclusions	Uncertainty of the MCR-ALS Model
TDS-1 (Unmodified)	631, 858, 1183 and 1294 (PET)	716, 1230 (Polyisobutene)	No crystallization	0.35 %
TDS-1 (Die-Cut)	631, 858, 1183 and 1294 (PET)	716, 1230 (Polyisobutene)	No crystallization	0.05 %
TDS-2 (Unmodified)	631, 858, 1183 and 1294 (PET)	1439 (Polyacrylate)	No crystallization	1.04 %
TDS-2 (Die-Cut)	631, 858, 1183 and 1294 (PET)	1439 (Polyacrylate)	No crystallization	0.82 %
TDS-3 (Unmodified)	1295, 1415 (Polyolefin)	489, 709 (Silicone)	Crystals but no growth	1.23 %
TDS-3 (Die-Cut)	1295, 1415 (Polyolefin)	489, 709 (Silicone)	Crystals but no growth	0.84 %
TDS-4 (Unmodified)	631, 858, 1183 and 1294 (PET)	716, 925, 1230 (Polyisobutylene)	No crystallization	1.78 %
TDS-4 (Die-Cut)	631, 858, 1183 and 1294 (PET)	716, 925, 1230 (Polyisobutylene)	Crystal nucleation and growth	0.61 %

Hit-Quality-Index of estimated pure component spectra

Second pure component spectra of all TDS samples studied here are demonstrated in Figure 5a. Even though all of the second components present the signature fentanyl peak at 1001 cm^{-1}, only unmodified and die-cut TDS-3 and die-cut TDS-4 had pure components that were similar to reference standard (USP) fentanyl in Raman signatures. To quantitatively evaluate our statistical analysis, hit-quality-index (HQI) values were calculated for each of the estimated pure components that were generated with the MCR-ALS model (Figure 5b) using the following equation

$$\mathrm{HQI} = \left[\vec{S} \cdot \vec{F}\right]^2 / \left[(\vec{S})^2 (\vec{F})^2\right] \quad (2)$$

where $\vec{S}$ is the vector representing the mean centered second component spectrum and $\vec{F}$ is the vector representing the mean centered spectrum of reference standard (USP) fentanyl.[69] This correlative method provides values between 0 and 1 with larger values indicating a higher correlation between the standard and the unknown and has been employed in spectroscopic analysis previously.[70] Here, the estimated component spectra was treated as the unknown and fentanyl as the standard. MCR-ALS analysis provided pure component spectra for both of the TDS-3 samples and die-cut TDS-4 with HQI values higher than 0.95 (Figure 5b). Note that 0.95 is commonly employed as a pass-fail threshold for analysis of unknown samples.[48]

The reference standard fentanyl spectrum was used in calculating the HQI values in this section and for comparison purposes throughout this study. The Raman mapping technique developed here did not require the reference standard Raman spectrum of fentanyl for identification but provided fentanyl spectra that was verified by quantitative methods. Recall that the absence of a crystallization inhibitor such as octyldodecanol in polyisobutylene adhesive could account for nucleation and growth of crystals in TDS-4. Also, stable crystals observed in

TDS-3 could be an inadvertent result of the manufacturing process. Finally, considering the large number of fentanyl analogs and other organic molecules with identical predominant Raman bands,[60] the significance of the HQI correlation of the crystal formed or otherwise observed in fentanyl TDS can be recognized as it provides robust and precise identification.

Conclusions

In summary, the capability of confocal Raman microscopic mapping coupled with MCR-ALS to characterize crystallization in complex TDS with off-label modifications, such as cutting TDS to attain smaller doses, was demonstrated. Here, such off-label modifications were simulated *via* die-cutting where the drug-in-adhesive layer was exposed to ambient conditions by a fresh edge. In certain TDS samples, fentanyl crystallization was observed as a result of this off-label modification which allowed for the potential of this Raman mapping method to be demonstrated. Utilizing multivariate curve resolution to assist confocal Raman mapping coupled with a correlative HQI library approach, crystals in fentanyl transdermal delivery systems could be visualized and their physio-chemical features could be thoroughly identified without *a priori* knowledge regarding the peak positions. Elicitation of pure spectral information could be achieved with the help of the MCR-ALS method implemented in this study. A broader implication is that, comprehensive assessment of the API distributions and formation of crystals and cocrystals in TDS can be performed *via* Raman mapping. Also, Raman mapping with MCR-ALS can be fit-for-purpose for formulation microstructure (Q3) sameness evaluation to support TDS product development.

Conflicts of interest

There are no conflicts to declare.

Acknowledgements

This project was supported, in part, by an appointment (H.Y. and T.X.) to the Research Participation Program at the Center for Drug Evaluation and Research administered by the Oak Ridge Institute for Science and Education through an interagency agreement between the U.S. Department of Energy and the U.S. Food and Drug Administration.

We would also like to acknowledge Sam G. Raney from FDA/CDER/Office of Generic Drugs (OGD)/Office of Research and Standards (ORS)/Division of Therapeutic Performance (DTP) for his valuable insight in discussions related to this project.

References

1. J. Breitenbach, W. Schrof and J. Neumann, *Pharmaceutical Research*, 1999, **16**, 1109-1113.
2. B. Vajna, H. Pataki, Z. Nagy, I. Farkas and G. Marosi, *International Journal of Pharmaceutics*, 2011, **419**, 107-113.
3. E. Widjaja, W. L. Lee and S. C. J. Loo, *Analytical Chemistry*, 2010, **82**, 1277-1282.
4. L. Sievens-Figueroa, A. Bhakay, J. I. Jerez-Rozo, N. Pandya, R. J. Romañach, B. Michniak-Kohn, Z. Iqbal, E. Bilgili and R. N. Davé, *International Journal of Pharmaceutics*, 2012, **423**, 496-508.
5. B. Gotter, W. Faubel and R. H. H. Neubert, *European Journal of Pharmaceutics and Biopharmaceutics*, 2010, **74**, 14-20.
6. N. A. Belsey, N. L. Garrett, L. R. Contreras-Rojas, A. J. Pickup-Gerlaugh, G. J. Price, J. Moger and R. H. Guy, *Journal of Controlled Release*, 2014, **174**, 37-42.
7. K. Wang, D.-W. Sun, Q. Wei and H. Pu, *LWT*, 2018, **96**, 66-74.
8. D. F. d. Andrade, B. Vukosavljevic, E. V. Benvenutti, A. R. Pohlmann, S. S. Guterres, M. Windbergs and R. C. R. Beck, *Pharmaceutical Development and Technology*, 2018, **23**, 414-425.
9. L. Franzen and M. Windbergs, *Advanced Drug Delivery Reviews*, 2015, **89**, 91-104.
10. C. L. Armstrong, H. G. M. Edwards, D. W. Farwell and A. C. Williams, *Vibrational Spectroscopy*, 1996, **11**, 105-113.
11. A. M. Wokovich, S. Prodduturi, W. H. Doub, A. S. Hussain and L. F. Buhse, *European Journal of Pharmaceutics and Biopharmaceutics*, 2006, **64**, 1-8.
12. A. F. Davis and J. Hadgraft, *International Journal of Pharmaceutics*, 1991, **76**, 1-8.
13. M. A. Pellett, A. F. Davis and J. Hadgraft, *International Journal of Pharmaceutics*, 1994, **111**, 1-6.
14. K. Moser, K. Kriwet, Y. N. Kalia and R. H. Guy, *International Journal of Pharmaceutics*, 2001, **224**, 169-176.
15. P. Santos, M. Machado, A. C. Watkinson, J. Hadgraft and M. E. Lane, *International Journal of Pharmaceutics*, 2009, **377**, 70-75.
16. J. W. Mullin and O. Söhnel, *Chemical Engineering Science*, 1977, **32**, 683-686.
17. M. N. Pastore, Y. N. Kalia, M. Horstmann and M. S. Roberts, *British journal of pharmacology*, 2015, **172**, 2179-2209.
18. P. Santos, A. C. Watkinson, J. Hadgraft and M. E. Lane, *International Journal of Pharmaceutics*, 2011, **416**, 155-159.
19. UCB, Request to initiate Neupro® down-titration Dear Healthcare Provider letter, www.ucb-group.com, (accessed March 21, 2008).
20. Enforcement Report for June 6, 2012, http://www.fda.gov/Safety/Recalls/EnforcementReports/ucm307229.htm, (accessed February 14, 2013).
21. F. Cilurzo, P. Minghetti, A. Casiraghi, L. Tosi, S. Pagani and L. Montanari, *European Journal of Pharmaceutics and Biopharmaceutics*, 2005, **60**, 61-66.
22. P. Jain and A. K. Banga, *Pharmaceutical Research*, 2013, **30**, 562-571.
23. P. Jain and A. K. Banga, *International Journal of Pharmaceutics*, 2010, **394**, 68-74.
24. S. Latsch, T. Selzer, L. Fink, M. Horstmann and J. Kreuter, *European Journal of Pharmaceutics and Biopharmaceutics*, 2004, **57**, 397-410.
25. S. Latsch, T. Selzer, L. Fink and J. Kreuter, *European Journal of Pharmaceutics and Biopharmaceutics*, 2004, **57**, 383-395.
26. S. Latsch, T. Selzer, L. Fink and J. Kreuter, *European Journal of Pharmaceutics and Biopharmaceutics*, 2003, **56**, 43-52.
27. R. Lipp and A. Muller-Fahrnow, *European Journal of Pharmaceutics and Biopharmaceutics*, 1999, **47**, 133-138.

28. R. Lipp, *Journal of Pharmacy and Pharmacology*, 1998, **50**, 1343-1349.
29. P. Minghetti, F. Cilurzo, S. Pagani, A. Casiraghi, R. Assandri and L. Montanari, *Pharmaceutical Development and Technology*, 2007, **12**, 239-246.
30. V. Sachdeva, Y. Bai, A. Kydonieus and A. K. Banga, *International Journal of Pharmaceutics*, 2013, **441**, 9-18.
31. M. Schulz, B. Fussnegger and R. Bodmeier, *European Journal of Pharmaceutical Sciences*, 2010, **41**, 675-684.
32. N. E. Variankaval, K. I. Jacob and S. M. Dinh, *Journal of Materials Science-Materials in Medicine*, 2002, **13**, 271-280.
33. N. E. Variankaval, K. I. Jacob and S. M. Dinh, *Journal of Biomedical Materials Research*, 1999, **44**, 397-406.
34. WO1999015156 B1, 1998.
35. N. Colthup, *Introduction to infrared and Raman spectroscopy*, Elsevier, 2012.
36. K. C. Gordon and C. M. McGoverin, *International Journal of Pharmaceutics*, 2011, **417**, 151-162.
37. G. P. S. Smith, C. M. McGoverin, S. J. Fraser and K. C. Gordon, *Advanced Drug Delivery Reviews*, 2015, **89**, 21-41.
38. A. V. Ewing and S. G. Kazarian, *Spectrochimica Acta Part A: Molecular and Biomolecular Spectroscopy*, 2018, **197**, 10-29.
39. H. Mitsutake, S. R. Castro, E. de Paula, R. J. Poppi, D. N. Rutledge and M. C. Breitkreitz, *International Journal of Pharmaceutics*, 2018, **552**, 119-129.
40. S. Šašić, *Applied Spectroscopy*, 2007, **61**, 239-250.
41. A. Balogh, G. Drávavölgyi, K. Faragó, A. Farkas, T. Vigh, P. L. Sóti, I. Wagner, J. Madarász, H. Pataki, G. Marosi and Z. K. Nagy, *Journal of Pharmaceutical Sciences*, 2014, **103**, 1278-1287.
42. D. R. Y. Willett, H.; Wokovich, A. M.; Rodriguez, J. D., , *American Pharmaceutical Review*, 2019, **22**, 48-51.
43. U. Helbig, *J. Cryst. Growth*, 2008, **310**, 2863-2870.
44. P. T. M. Cheng and P. Hawley, *Journal of Palliative Medicine*, 2017, **20**, 1311-1312.
45. M. Lee and J. Phillips, *Drug Topics*, 2002.
46. J. Huynh and C. Aebi, *Oregon DUR Board Newsletter*, 2008, **10**.
47. A. Abbas, L. Tian, J. J. Morrissey, E. D. Kharasch and S. Singamaneni, *Adv Funct Mater*, 2013, **23**, 1789-1797.
48. C. M. Gryniewicz-Ruzicka, J. D. Rodriguez, S. Arzhantsev, L. F. Buhse and J. F. Kauffman, *Journal of Pharmaceutical and Biomedical Analysis*, 2012, **61**, 191-198.
49. A. Henderson, *Zenodo*, (2017, April 6).
50. S. D. Roy, M. Gutierrez, G. L. Flynn and G. W. Cleary, *Journal of Pharmaceutical Sciences*, 1996, **85**, 491-495.
51. K. L. Ulman and C. L. Lee, *Journal of Controlled Release*, 1989, **10**, 273-281.
52. 2003.
53. C. Y. Liang and S. Krimm, *Journal of Molecular Spectroscopy*, 1959, **3**, 554-574.
54. F. de Buyl, *International Journal of Adhesion and Adhesives*, 2001, **21**, 411-422.
55. L. Jayes, A. P. Hard, C. Séné, S. F. Parker and U. A. Jayasooriya, *Analytical Chemistry*, 2003, **75**, 742-746.
56. Y. V. Zavgorodnev, E. Sagitova, G. Y. Nikolaeva, K. Prokhorov, P. Pashinin, L. Novokshonova, T. Ushakova, E. Starchak and E. Antipov, 2012.
57. J. J. Higgins, F. C. Jagisch and N. E. Stucker, *Handbook of Pressure Sensitive Adhesive Technology II*, Van Nostrand Reinhold, New York, 1989.
58. H. S. Tan and W. R. Pfister, *Pharm Sci Technol To*, 1999, **2**, 60-69.

59. N. Roohpour, J. M. Wasikiewicz, A. Moshaverinia, D. Paul, I. U. Rehman and P. Vadgama, *Materials*, 2009, **2**, 719-733.
60. J. Omar, B. Slowikowski, C. Guillou, F. Reniero, M. Holland and A. Boix, *Journal of Raman Spectroscopy*, 2019, **50**, 41-51.
61. J. Jaumot, R. Gargallo, A. de Juan and R. Tauler, *Chemometrics and Intelligent Laboratory Systems*, 2005, **76**, 101-110.
62. J. Felten, H. Hall, J. Jaumot, R. Tauler, A. de Juan and A. Gorzsás, *Nature Protocols*, 2015, **10**, 217.
63. M. B. Mamián-López and R. J. Poppi, *Microchemical Journal*, 2015, **123**, 243-251.
64. A. C. d. O. Neves, R. Tauler and K. M. G. de Lima, *Analytica Chimica Acta*, 2016, **937**, 21-28.
65. R. Tauler, *Chemometrics and Intelligent Laboratory Systems*, 1995, **30**, 133-146.
66. R. Tauler, A. Smilde and B. Kowalski, *Journal of Chemometrics*, 1995, **9**, 31-58.
67. N. B. Gallagher, J. M. Shaver, E. B. Martin, J. Morris, B. M. Wise and W. Windig, *Chemometrics and Intelligent Laboratory Systems*, 2004, **73**, 105-117.
68. J. M. I. Kenneth, S. K. Govil and K. S. Bhatia, *Journal*, 2009.
69. S. Lee, H. Lee and H. Chung, *Analytica Chimica Acta*, 2013, **758**, 58-65.
70. J. D. Rodriguez, B. J. Westenberger, L. F. Buhse and J. F. Kauffman, *Analytical Chemistry*, 2011, **83**, 4061-4067.

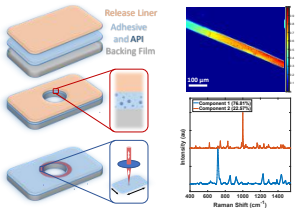

Raman mapping and chemometric models were used to characterize crystal formation in fentanyl transdermal delivery systems resulting from off-label modifications.